

Predicting Benzene Fluxes in NaX Membranes from Atomistic Simulations of Cooperative Diffusivities

Harikrishnan Ramanan,^{†,‡} Scott M. Auerbach,^{*,†,§} and Michael Tsapatsis^{*,†,‡}

Departments of Chemical Engineering and of Chemistry, University of Massachusetts, Amherst, Massachusetts 01003, and Department of Chemical Engineering and Materials Science, University of Minnesota, Minnesota 55455

Received: June 2, 2004; In Final Form: August 11, 2004

In the preceding companion article, we reported high-temperature molecular dynamics (MD) simulations to trace single-molecule as well as collective mean square displacements over a range of temperatures (600–1500 K) and loadings (infinite dilution to four benzenes per supercage) to evaluate respectively the self-diffusivities and cooperative (alternatively Maxwell–Stefan) diffusivities of benzene in NaX (Si:Al = 1.2). In this follow-up article, we use the loading- and temperature-dependent Maxwell–Stefan diffusivities to predict single-component fluxes for benzene in NaX membranes at steady state as a function of typical experimental parameters such as temperature, benzene feed side and permeate side partial pressures. We explore whether support resistances need to be included in our transport model. We compare our model predictions with experimental permeation data and find that our MD-simulated diffusivities overestimate experimental fluxes by about 2 orders of magnitude when support resistance is ignored. On the other hand, when support resistances are included, our predictions come within 1 order of magnitude of experimental data. The remaining discrepancy, which is analogous to those between microscopic and macroscopic probes of diffusion in zeolites, may arise from defects within zeolite membranes.

I. Introduction

Modeling sorbate transport through zeolite membranes has been of considerable research interest in recent times.^{1–29} Studies on membrane-based separations are commonly focused on zeolites with simple compositions such as noncationic MFI zeolite (silicalite),^{1–4,6,7,9,11,17,22,23,28,30–34} whereas very few reports exist on cationic systems such as zeolite-A^{29,35–43} and FAU-type zeolites.^{5,18,19,23,44–49} Recent investigations have confirmed that FAU-type membranes (NaX and NaY) give fairly high separation efficiencies for hydrocarbon mixture separation.^{18,23,46–48,50} It has been commonly observed that the presence of benzene in the feed reduces the flux of saturated hydrocarbons such as cyclohexane, methyl pentane, or dimethylbenzene through FAU membranes.^{18,46,48} In such systems where motion is influenced by cations, interesting questions remain when seeking to explain membrane performance and selectivity from atomistic simulations. In this Article, we apply simulated diffusivities in a transport model to rationalize experimental benzene fluxes through NaX and NaY membranes.

Atomistic simulation studies of sorbate transport in zeolite crystals and membranes aid in answering the question: How do fundamental sorbate–zeolite and sorbate–sorbate interactions affect the interplay of sorption and diffusion, which in turn influence membrane permselectivity? Such modeling also aids in the computational screening of zeolite membranes as well as in the design of membrane systems, to meet specific separation requirements in industrial processes.^{4,14,22} One of the

most common of approaches is the use of membrane transport models based on the Fickian or Onsager⁵¹ (or equivalently Maxwell–Stefan) formulations to describe diffusion through zeolite membranes.^{52–57} Fick's law relates macroscopic fluxes to concentration gradients of the diffusing components, whereas Onsager's formulation uses the more fundamental chemical potential gradients to characterize fluxes. Due to the complicated physical interpretation of the Onsager transport coefficients, the equivalent Maxwell–Stefan approach, which was originally developed for multicomponent diffusion in bulk fluids, has been applied with great skill to diffusion in zeolites by Krishna and co-workers.^{58–60} The Fickian and Maxwell–Stefan (MS, alternatively cooperative) diffusivities (D_{Fick} and D^{MS} , respectively) are related through the thermodynamic correction factor, Γ , in the form $D_{\text{Fick}} = D^{\text{MS}}\Gamma$. The Fickian diffusivity is therefore interpreted to be inclusive of intermolecular drag effects (contributed by D^{MS}) and thermodynamic nonidealities (contributed by Γ).^{53,59,61–63} The above-mentioned formulations have been used to predict transport through membranes for several systems using (a) sorption isotherm data and (b) the loading-dependent cooperative (MS) diffusivities.^{16,54,55,64–67} In previous work from the Tsapatsis group, Nikolakis et al.¹⁸ reported Maxwell–Stefan modeling of benzene permeation through NaX membranes, fitting fluxes to loading-independent MS diffusivities. Such modeling is dissatisfying for several reasons. First, loading-independent MS diffusivities are characteristic of sorbates executing fluidlike motion in nanopores,⁵⁹ whereas benzene is known to exhibit jump diffusion among sites in FAU cages, and between cages in crystallites. As such, the underlying physics of loading-independent MS diffusivities should not apply to benzene motion through NaX membranes. Second, one would ultimately like to surmise the loading dependence of MS

* Address correspondence to these authors. E-mail: S.M.A., auerbach@chem.umass.edu; M.T., tsapatsi@cems.umn.edu.

[†] Department of Chemical Engineering, University of Massachusetts.

[‡] Department of Chemical Engineering and Materials Science, University of Minnesota.

[§] Department of Chemistry, University of Massachusetts.

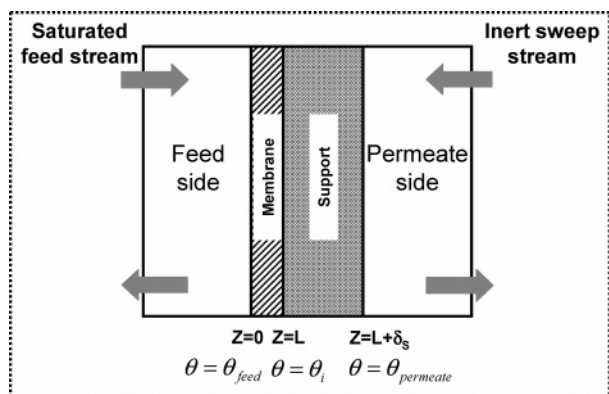


Figure 1. Schematic model representing steady-state transport of benzene through a supported NaX membrane.

diffusion from the temperature and pressure dependence of experimental membrane fluxes.

In the preceding companion paper, we performed high temperature molecular dynamics (MD) simulations of benzene in NaX to calculate the temperature and loading dependence of the self-diffusivities and cooperative diffusivities by keeping the cations in motion, thereby faithfully reproducing benzene motion in NaX. We also showed that our MD simulations estimate diffusivities and activation energies for self-diffusion, in excellent agreement with microscopic measurement techniques such as pulse field gradient (PFG) NMR and quasi-elastic neutron scattering (QENS). In this follow-up article, we apply these cooperative diffusivities of benzene in NaX from our MD simulations in a simple Fickian transport model to predict macroscopic membrane fluxes as a function of temperature, benzene feed side, and permeate side partial pressures. The Fickian diffusivity is a product of the cooperative diffusivity (calculated from our MD studies in the preceding companion article) and the thermodynamic factor (obtained from reported sorption isotherm data⁶⁸). This methodology does not impose on us (a) a particular loading dependence for the cooperative diffusivities, or (b) the use of Darken's approximation or facsimile, wherein the Fickian diffusivity is approximated as a product of the self-diffusivity and the thermodynamic factor.^{2,6,14,23,52,54–56}

The model we describe below accounts for transport resistance from sorbate motion inside zeolite pores and also from sorbate motion in the membrane support.^{69–71} We find below that including such support resistance is crucial for getting to within an order of magnitude of experimental benzene fluxes. We suggest that the remaining discrepancy arises from defects in the membrane and is analogous to discrepancies between microscopic and macroscopic probes of diffusion in zeolites.⁵⁹

In what follows, we discuss briefly in section II the transport model that describes benzene diffusion in a NaX membrane. We investigate in section III how single-component fluxes of benzene in NaX behave as a function of temperature, feed, and permeate side partial pressures and subsequently evaluate the usefulness of our model in predicting experimental flux measurements. In section IV, we evaluate the practical relevance of our model in predicting benzene fluxes at operating conditions employed in industrial separations. Finally, we discuss our conclusions and ensuing work in section V.

II. Modeling Steady State Transport of Benzene through NaX Membrane

Figure 1 shows the schematic representation of the Wicke–Kallenbach membrane permeation system used to model single-

component steady-state transport of benzene through a single-crystal NaX membrane supported by a porous alumina disk. The feed and permeate sides of the membrane-support composite are respectively in contact with a saturated stream of sorbate vapor (i.e., benzene saturated in helium inert at a specified temperature) and a sweep stream of inert gas (i.e., helium), to maintain a reasonable chemical potential gradient across the membrane thickness. The model assumes that (a) transport is in steady state, (b) benzene permeation occurs from a well-mixed upstream compartment to a well-mixed downstream compartment, (c) membrane transport occurs only through microporous zeolite diffusion (intracrystalline permeation), (d) codiffusion of helium through the membrane alongside benzene is neglected in view of the strong heat of adsorption of benzene in NaX (see preceding companion article), and (e) benzene and helium counter-diffusion through the support is characterized by molecular diffusion taking into account any convection induced by diffusion.

The inter-related Fickian and Onsager's (or Maxwell–Stefan) formulations have commonly been applied for describing sorbate transport through zeolite membranes.^{13,16,57,72,73} We therefore avoid a detailed repetition of the theory and recount some necessary definitions pertinent to our model development. The governing equation for representing steady-state benzene flux (N_B) through the membrane is given by

$$\frac{\partial N_B}{\partial Z} = \frac{\partial}{\partial Z} \left[D^{\text{MS}}(\theta, T) \Gamma(\theta) \frac{\partial \theta}{\partial Z} \right] = 0 \quad (1)$$

where

$D^{\text{MS}}(\theta, T)$: loading and temperature-dependent cooperative diffusivity (m^2/s)

θ : fractional sorbate loading with $\theta = \frac{\Theta}{\Theta_{\text{sat}}}$

Θ : molecular loading per unit cell (from adsorption isotherm data)

Θ_{sat} : saturation loading at a particular T

$\Gamma = \theta \left. \frac{\partial \ln p}{\partial \theta} \right|_T$: thermodynamic factor as a function of partial pressure (p) and loading

For the Langmuir adsorption isotherm,

$$\theta = \frac{\Theta}{\Theta_{\text{sat}}} = \frac{bp}{1 + bp} \quad (2a)$$

$$\Gamma(\theta) = \frac{1}{1 - \theta} \quad (2b)$$

where p (kPa) is the partial pressure of the gas phase in equilibrium with the adsorbed phase in the zeolite and $b(T)$ is the sorption equilibrium constant (kPa^{-1}) for benzene in NaX.

Using the appropriate boundary conditions corresponding with the experimental conditions, we have

$$Z = 0 \quad \theta = \theta_{\text{feed}} \quad (3)$$

$$Z = L \quad \theta = \theta_i \quad (4)$$

where L is the membrane thickness and θ_i is the fractional loading at the membrane-support interface.

As noted above, our model assumes transport through the support to occur by molecular diffusion, and not by flow. Taking into account the counter-diffusive flux of helium (N_{He}) through the support from the permeate side of the membrane—support composite, the partial pressure gradient across the support ($\partial p_s/\partial z$) is related to the steady-state flux of benzene (N_B) in the form^{69,70}

$$N_B = \frac{\epsilon_s D_{B,\text{He}}}{\tau(1-y)} \times \frac{1}{RT} \left(-\frac{\partial p_s}{\partial z} \right) - \frac{y N_{\text{He}}}{1-y} \quad (5)$$

where y is the benzene mole fraction in the sweep stream mixture, ϵ_s is the support porosity, and $D_{B,\text{He}}$ the molecular diffusivity of benzene in helium estimated from Fuller's correlation.⁷⁴ Equation 5 is a sufficient condition for describing transport through the support when the total pressure is constant across the membrane-support composite. The benzene loading at the permeate side of the membrane—support composite is given by

$$Z = L + \delta_s \quad \theta = \theta_{\text{permeate}} \quad (6)$$

where δ_s is the thickness of the support.

By simultaneously solving eqs 1 and 5 using the boundary conditions in eqs 3, 4, and 6, we obtain the predicted flux of benzene, N_B , the benzene partial pressure at the membrane—support interface, p_i and henceforth the true pressure drop across the membrane, $p_{\text{feed}} - p_i$, for given conditions of T , p_{feed} , and p_{permeate} . A typical value of $L = 15 \mu\text{m}$ and $\delta_s = 2.1 \text{ mm}$ has been considered in our model calculations.¹⁸ When eq 5 is used to describe permeation measurements through the bare support under conditions identical to those of the membrane permeation experiments (with benzene and helium counter-diffusing across the support), an approximately constant value of $\tau/\epsilon = 33.25$, i.e., $\tau = 6.65$ for $\epsilon_s = 0.2$ is obtained, which subsequently is used to determine the flux in the presence of the membrane. A high value of $\tau/\epsilon = 33.25$ indicates that the supports used in the experiments¹⁸ offer significant resistance to benzene transport.

The solution of eqs 1 and 5 above requires (a) sorption data to evaluate Γ and (b) molecular dynamics data (see preceding paper) to evaluate $D^{\text{MS}}(\theta, T)$. The temperature range is chosen to be 338.15–433.15 K (typical range for experimental flux measurements^{18,47}). The thermodynamic factor (Γ) is evaluated by extrapolating Ruthven and Doetsch's experimental sorption data for benzene in NaX⁶⁸ to the temperatures of interest. The available sorption data are found to fit well to a Langmuir adsorption isotherm (eqs 2a and 2b), thereby enabling an Arrhenius type of fit for $b(T)$ ^{59,75} and a linear temperature dependence for $\Theta_{\text{sat}}(T)$. The temperature dependence of $\Theta_{\text{sat}}(T)$ could be interpreted by the explanation that, if the partial molar volume increases with temperature, while the cage volume is more nearly constant with temperature, the number of sites = (cage volume/volume of guest) will decrease with temperature, as is seen. From these approximations, the Langmuir model parameters corresponding to the temperatures of interest in the membrane experiments are determined. Though one may expect that Θ_{sat} for sorbates in zeolites should be independent of temperature because the total number of sorption sites in a zeolite is a constant, a weak dependence on temperature is confirmed for Θ_{sat} from the experimental data of Ruthven and Doetsch.⁶⁸ This temperature dependence likely arises because the partial molar volume of the adsorbed phase is not constant, though the pore volume is nearly constant. In Figure 2, we show

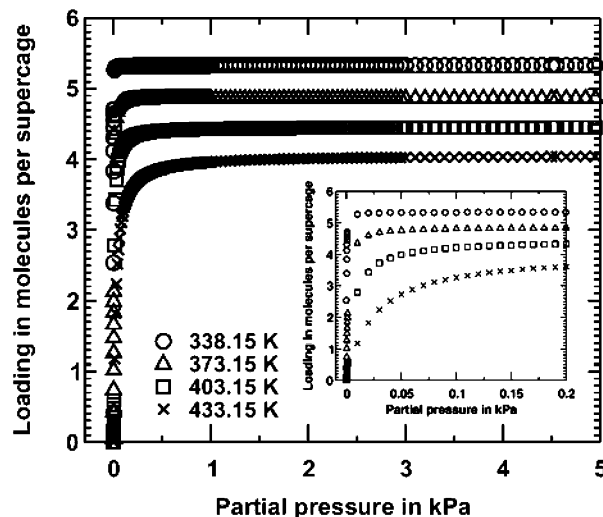


Figure 2. Adsorption equilibria for benzene in NaX⁶⁸ fitted to the Langmuir form.

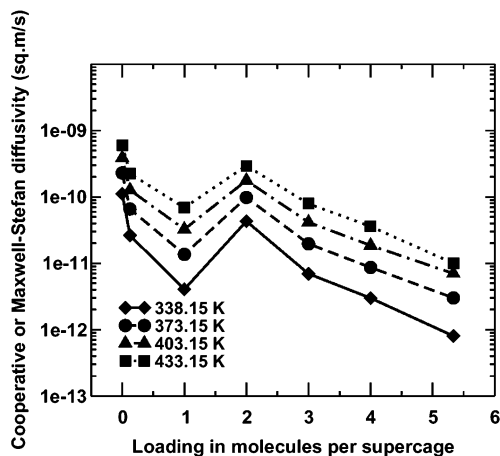


Figure 3. Loading dependence of the cooperative diffusivities of benzene in NaX extrapolated to temperatures of interest.

the adsorption isotherms for benzene in NaX at the temperatures of interest extrapolated from the data of Ruthven and Doetsch.⁶⁸

We extrapolate $D^{\text{MS}}(\theta)$ at each T of interest on the basis of the Arrhenius temperature dependence of D^{MS} found from our MD simulations of benzene in NaX (see preceding companion paper). Figure 3 shows the extrapolated cooperative diffusivity isotherms. Our MD simulations cover the range of loadings from $\Theta = \text{infinite dilution}$ to four benzenes per supercage. The cooperative diffusivities for the loading of five molecules per supercage have been obtained from linear extrapolation on the semilog plot (Figure 3) based on the monotonic decrease in the cooperative diffusivity for $\Theta > 2$. The solution procedure is further simplified by using approximate analytical expressions for $D^{\text{MS}}(\theta)$ by linear interpolation so as to obtain an analytical expression for N_B in eq 1. In addition, as N_B and N_{He} are constant for steady-state transport, eq 5 also reduces to an algebraic expression. As p_i (and therefore θ_i) is unknown, an iterative scheme is used to solve the coupled algebraic equations.

It is clear from eq 1 that the flux depends on several factors: $\Theta_{\text{sat}}(T)$, $D^{\text{MS}}(\theta, T)$, $\Gamma(\theta)$, and the net driving force across the membrane thickness, $\Delta\Theta_{\text{net}} = \Theta_{\text{feed}} - \Theta_i$. To test the usefulness of the transport model, we first consider the steady-state flux predictions of benzene through NaX as a function of typical experimental variables such as temperature (T), benzene feed partial pressure (p_{feed}), and benzene permeate partial pressure (p_{permeate}). To capture the effect of the loading dependence of

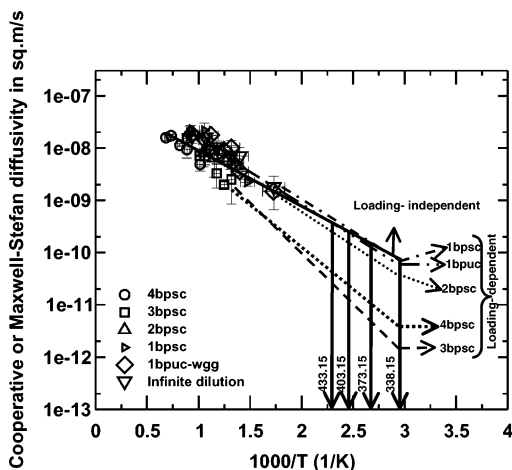


Figure 4. Extrapolation of cooperative or Maxwell–Stefan diffusivities for benzene in NaX from high-temperature MD simulations using the Arrhenius temperature dependence for the loading-dependent and loading-independent models.

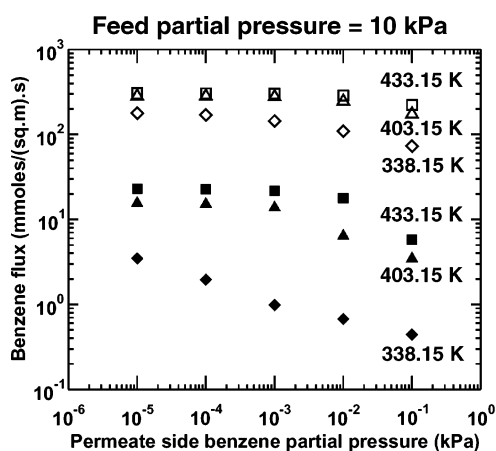


Figure 5. Prediction of benzene flux as a function of permeate partial pressure (p_{permeate}) by the loading-dependent (\blacklozenge , \blacktriangle , \blacksquare) and the loading-independent models (\diamond , Δ , \square) for $p_{\text{feed}} = 10$ kPa and $T = 338.15$, 403.15 , and 433.15 K, respectively.

the cooperative diffusivity on the membrane flux, the model predictions with a loading-independent cooperative diffusivity model (based on $D^{\text{MS}}(T)$) are also plotted for comparison. These $D^{\text{MS}}(T)$ shown in Figure 4 are based on an “all-loading” average of our high temperature MD, extrapolated using the Arrhenius temperature dependence (see preceding companion paper). Further, we compare our model predictions with available experimental data on NaX and NaY membranes. In view of limited availability of experimental flux measurements across bare supports, we considered support resistance in our model only when comparing our model predictions with the experimental fluxes of Nikolakis et al.¹⁸ Henceforth, in sections III.A–C and IV below, $\Delta\Theta_{\text{net}} = \Theta_{\text{feed}} - \Theta_{\text{permeate}}$ represents the concentration drop across the membrane.

III. Results and Discussion

A. Effect of Permeate Side Partial Pressure. Figures 5 and 6 show the effect of p_{permeate} on the benzene flux across a $15 \mu\text{m}$ thick membrane for $T = 338.15$ – 433.15 K and $p_{\text{feed}} = 10$ kPa and 5×10^{-3} kPa, respectively. For a fixed p_{feed} and T , the increase in p_{permeate} results in a decrease in the net diffusion driving force across the membrane i.e., $\Delta\Theta_{\text{net}}$, thereby imparting a corresponding decrease in the benzene flux across the membrane. This behavior is countered to some extent by the

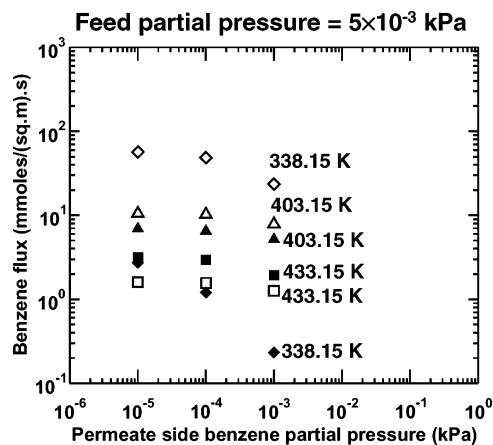


Figure 6. Prediction of benzene flux as a function of permeate partial pressure (p_{permeate}) by the loading-dependent (\blacklozenge , \blacktriangle , \blacksquare) and the loading-independent models (\diamond , Δ , \square) for $p_{\text{feed}} = 5 \times 10^{-3}$ kPa and $T = 338.15$, 403.15 , and 433.15 K, respectively.

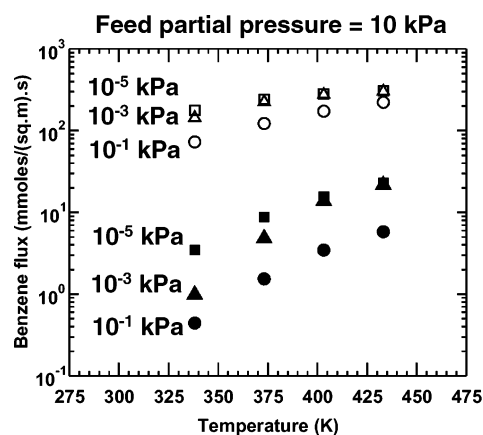


Figure 7. Prediction of benzene flux as a function of temperature by the loading-dependent (\blacksquare , \blacktriangle , \bullet) and the loading-independent models (\square , Δ , \circ) for $p_{\text{feed}} = 10$ kPa and $p_{\text{permeate}} = 10^{-5}$, 10^{-3} , and 10^{-1} kPa, respectively.

tendency of thermodynamic factor $\Gamma(\theta)$ to increase the flux with p_{permeate} due to the increase in the equilibrium adsorption loading of benzene. However, the driving force effect prevails in determining the overall flux behavior under the conditions investigated above. The fluxes predicted by the loading-independent $D^{\text{MS}}(T)$ model exhibit a dependence similar to that of the loading-dependent $D^{\text{MS}}(T, \theta)$ case, suggesting that the effect of the loading dependence of the D^{MS} is not significant under these conditions. However, the disparities in the flux predictions between these models originate from the disparities in the magnitudes of the loading-independent and loading-dependent MS diffusivities extrapolated from MD (Figure 4).

B. Effect of Temperature. Figures 7 and 8 show the effect of T (in the range $T = 338.15$ – 433.15 K) on the benzene flux across a $15 \mu\text{m}$ thick membrane for $p_{\text{permeate}} = 10^{-5}$ to 10^{-1} kPa while $p_{\text{feed}} = 10$ kPa and 5×10^{-3} kPa, respectively. The increase in the benzene flux with temperature for $p_{\text{feed}} = 10$ kPa is due to the activated nature of diffusion, resulting in an order of magnitude increase in D^{MS} from 338.15 to 433.15 K. This effect is countered by the tendency of Γ and $\Theta_{\text{sat}}(T)$ to decrease the flux with temperature, due to a decrease in benzene loading with temperature. For $p_{\text{feed}} = 5 \times 10^{-3}$ kPa, the effect of Γ and $\Theta_{\text{sat}}(T)$ becomes more significant and when these competing effects balance each other, a flux maximum is obtained (Figure 8). The fluxes predicted by the loading-independent $D^{\text{MS}}(T)$ model decrease with temperature when p_{feed}

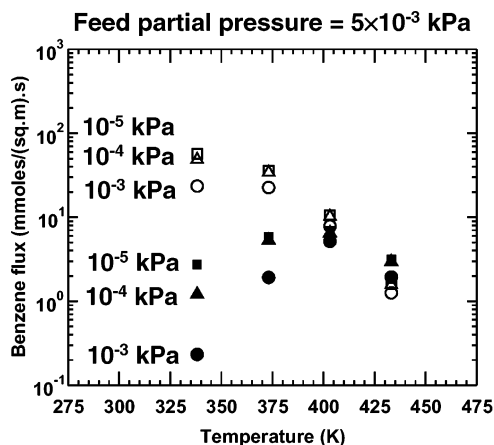


Figure 8. Prediction of benzene flux as a function of temperature by the loading-dependent (■, ▲, ●) and the loading-independent models (□, △, ○) for $p_{\text{feed}} = 5 \times 10^{-3}$ kPa and $p_{\text{permeate}} = 10^{-5}$, 10^{-4} , and 10^{-3} kPa, respectively.

$= 5 \times 10^{-3}$ kPa due to the dominance of the Γ and $\Theta_{\text{sat}}(T)$ effects over the activated diffusion effect.

C. Effect of Feed Partial Pressure. In Figure 9, we show the influence of benzene feed partial pressure on the membrane flux for $p_{\text{permeate}} = 10^{-5}$ kPa and $T = 373.15$ K. An approximately constant flux of benzene is predicted across the membrane by the loading-dependent $D^{\text{MS}}(T, \theta)$ model for $p_{\text{feed}} = 5 \times 10^{-3}$ to 10 kPa. This result suggests that a significant driving force across a NaX zeolite membrane is sufficient to obtain a reasonable benzene flux, i.e., $O(10 \text{ mmol}/(\text{m}^2 \cdot \text{s}))$, comparable to that measured in polymeric membranes under similar operating conditions. In view of their high fluxes, polymeric membranes are more strongly advocated for specific industrial applications (i.e., saturated–unsaturated hydrocarbon separations)^{76–92} than zeolite membranes. We hope our model predictions contribute favorably toward the application of zeolite membrane technology. Such fluxes in Figure 9 are also contributed by the “close-to-saturation” feed side loadings for the range $p_{\text{feed}} = 5 \times 10^{-3}$ to 10 kPa (Figure 2). The relatively stronger dependence of the flux on p_{feed} for the loading-independent model as compared to the loading-dependent one (Figure 9) arises from the nonmonotonic loading dependence of the diffusion isotherm (Figure 3) and the disparities in the magnitudes of the extrapolated diffusivities between the models. In section IV below, we touch upon the economic importance of the membrane flux at industrially relevant conditions in greater detail.

D. Prediction of Experimental Membrane Fluxes. In Figure 10, we show how our model predictions compare with the experimental fluxes of benzene in NaX membranes supported on porous alumina disks reported by Nikolakis et al.¹⁸ The benzene loadings at the membrane–support interface determined from solving eqs 1 and 5 are shown in the adjoining table in Figure 10 along with the feed side and permeate side loadings. We note that the experimental data we attempt to model reveal a limited range of benzene loadings across the membrane thickness. In particular, in all cases the loading exceeds 2.74 molecules per supercage. At the lowest temperature, the loading drop across the membrane–support composite is only 0.043 molecules per supercage, whereas at the highest temperature the loading drop reaches 1.32 molecules per supercage. If we ignore support resistance, the loading- and temperature-dependent $D^{\text{MS}}(\theta, T)$ generated by MD overestimate the experimental fluxes by about 2 orders of magnitude. On the other hand, including support resistance brings the model predictions to

within 1 order of magnitude agreement. In both cases, the transport model captures the temperature dependence of flux reasonably well, nevertheless overpredicting the experimental measurements (vide infra).

In Figure 11, we compare our model predictions with the experimental fluxes of benzene in NaY membranes supported on tubular porous alumina supports reported by Morooka and co-workers.^{46,47} In the absence of sufficient benzene sorption isotherm data on NaY, the Langmuir adsorption parameters for benzene–NaX are assumed to be valid for benzene–NaY as well. We did not include support resistance in our treatment of benzene permeation through NaY membranes, because we could not obtain sufficient information about the supports used in these experiments.^{46,47} Figure 11 shows that our model (without support resistance) overpredicts the experimental fluxes for benzene in NaY, also within an order of magnitude. It remains to be seen whether this level of agreement for benzene in NaY membranes arises from fortuitous cancellation of errors, or not. Nonetheless, these comparisons demonstrate the qualitative success of the transport model equipped with our MD-simulated MS diffusivities. Such a reasonable agreement (within an order of magnitude) with experiments performed on membranes synthesized under different experimental conditions is noteworthy.

Here we speculate on the remaining discrepancy between simulated and measured benzene fluxes through faujasite-type zeolites. The remaining discrepancy may be attributed to inaccuracies in simulated diffusivities, extrapolation of adsorption isotherms and also to possible experimental artifacts. Here we discuss these possibilities. First, regarding the simulated diffusivities, they may be in error because of errors in the underlying force field. However, in the preceding companion paper, we show that the loading and temperature dependencies of self-diffusion are captured accurately with this force field. A more likely source of simulation error is the method used to extrapolate high-temperature diffusivities to low temperatures, and the approach for extrapolating the loading dependence beyond 4 molecules per cage. The latter extrapolation was necessary because of the mismatch between simulated loadings (up to 4 molecules per supercage) and experimental loadings in permeation measurements (2.74–5.33 molecules per supercage in the experiments of Nikolakis et al.¹⁸ and 3.8–4.56 molecules per supercage in the experiments of Morooka and co-workers^{46,47}). It is not obvious, though, that such extrapolations should lead to simulated fluxes consistently overestimating experimental fluxes by an order of magnitude.

Second, the use of isotherm data extrapolated from experimental adsorption isotherms may contribute as a source of error. A fully consistent simulation approach requires the prediction of adsorption isotherms from the potential used to derive the dynamics. We plan to investigate this aspect as part of our future work. Another possibility involves experimental artifacts. In particular, though our MD simulations model diffusion through single-crystal NaX because we use periodic boundary conditions, the experimental fluxes result from permeation through polycrystalline membranes, with grain boundaries, blocked pores, tortuous diffusion paths, and possibly, strong extracrystalline adsorption sites. It is straightforward to see how additional transport resistances from such disorder patterns can reduce fluxes from single-crystal values. The disagreement in the diffusivities is quite reminiscent of the well-documented discrepancies between macroscopic and microscopic measurements of diffusion,⁵⁹ where microscopic diffusivities often exceed macroscopic ones by one or more orders of magnitude. (For

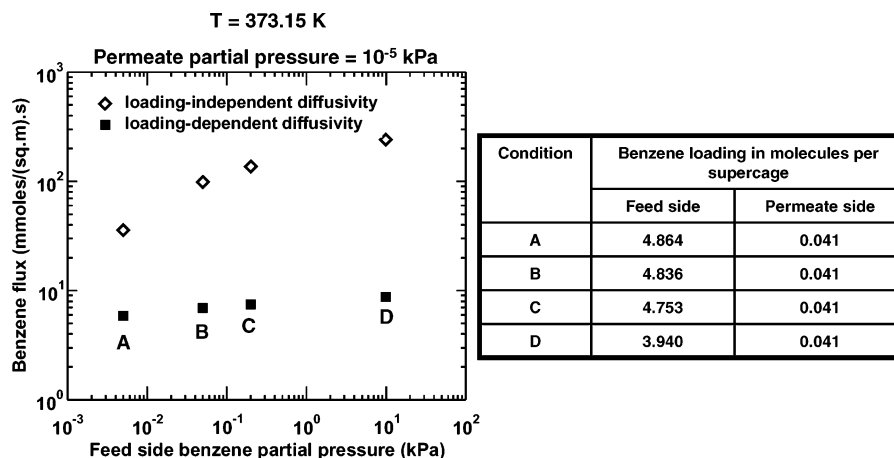


Figure 9. Prediction of benzene flux as a function of feed partial pressure by the loading-dependent and the loading-independent models for $T = 373.15$ K and $p_{\text{permeate}} = 10^{-5}$ kPa. The adjoining table shows the respective benzene loadings on the feed and permeate sides of the membrane.

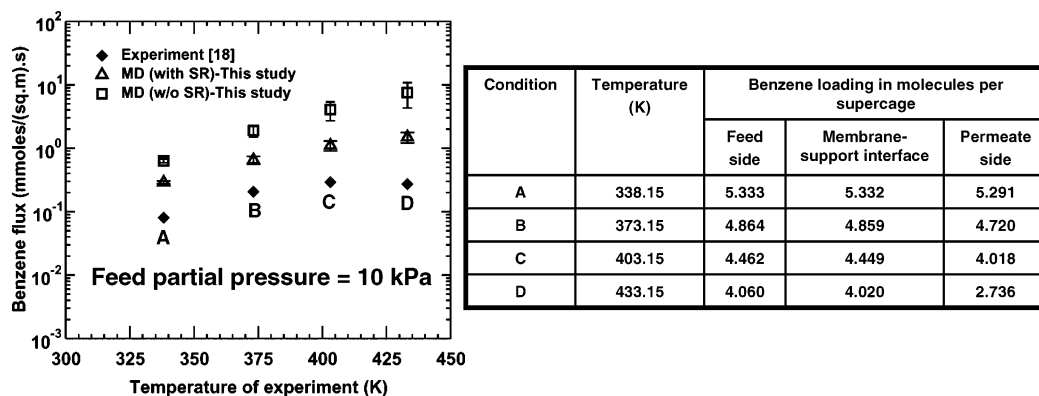


Figure 10. Comparison of experimental¹⁸ and simulated (this study) fluxes of benzene in NaX, with support resistance (with SR) and without support resistance (w/o SR). The adjoining table shows the respective benzene loadings on the feed side, membrane-support interface and permeate side of the membrane. Error bars shown for our MD results are occasionally found to be smaller than the size of legend symbols used.

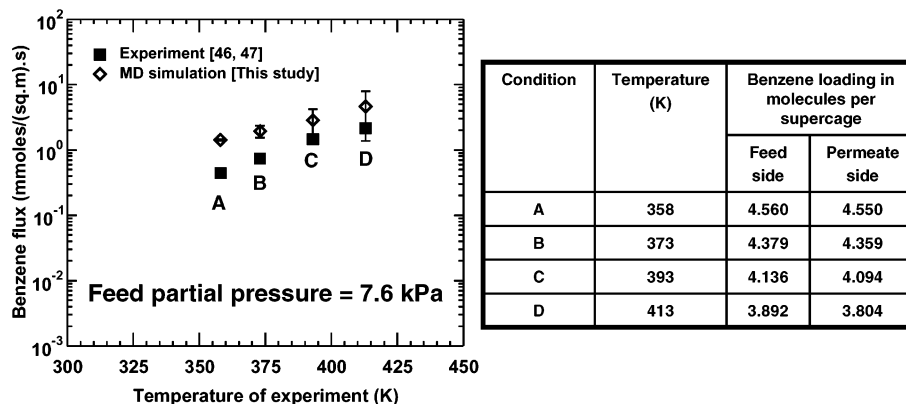


Figure 11. Comparison of experimental^{46,47} and simulated (this study) fluxes of benzene in NaY. The adjoining table shows the respective benzene loadings on the feed and permeate sides of the membrane. Error bars shown for our MD results are occasionally found to be smaller than the size of legend symbols used.

benzene in NaX, the discrepancy between the loading dependencies measured by pulsed field gradient (PFG) NMR and tracer zero-length column data is well-known.⁹³ We thus suggest that the remaining discrepancy between predicted and experimental benzene fluxes through NaX membranes (Figures 10 and 11) provides yet another example of the macroscopic–microscopic divide that persists in the field of diffusion in zeolites.

IV. Model Extrapolation to Conditions of Interest in Industrial Separations

Research studies on membrane-based separation of close-boiling or azeotropic hydrocarbon mixtures (e.g., benzene–

cyclohexane, benzene–methanol, etc.) are mainly driven by the need to improve the process efficiency of conventional separation processes (e.g., extractive and azeotropic distillations) involving such mixtures. Numerous studies show that polymer-based^{76–92} and zeolite-based membranes^{18,50,94} provide economically attractive alternatives to the energy intensive conventional separation technologies. Factors that play an important role in the selection of the best performing membrane for a specific industrial separation requirement are flux or permeance, selectivity toward the desired product, feasibility of operation at industrially relevant conditions, membrane cost, reliability, robustness, ease of scale-up, and environmental and safety–

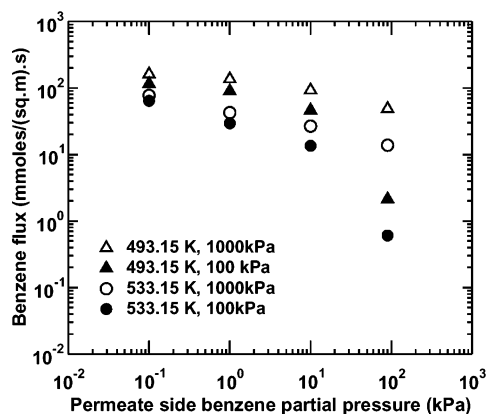


Figure 12. Prediction of benzene flux as a function of permeate partial pressure (p_{permeate}) by the loading-dependent model for conditions of interest in Industrial separations.

related issues. Laboratory studies on polymer-based^{76–92} and zeolite-based^{18,50,94} membranes are usually restricted to milder operating conditions (moderately lower temperatures and partial pressures). Several investigations demonstrate the potential application of polymer-based membranes in saturated-unsaturated hydrocarbon mixture separation involving benzene [refs 76–92 and citations therein]. Reported studies on Faujasite membranes^{18,50,94} and our flux predictions in section III show promise in suggesting that although fluxes of benzene are comparable between polymeric and zeolitic membranes, i.e., $O(0.01–10 \text{ mmol}/(\text{m}^2\cdot\text{s}))$ when $T = 298–433 \text{ K}$, Faujasite membranes provide higher selectivities ($\sim 10–180$)^{18,50,94} than polymeric membranes ($2–98.5$).^{76–92} In this perspective, extrapolating laboratory-based conclusions to industrially relevant operating conditions is important to assess the design feasibility of membrane-based technologies. The feasibility may be expressed in terms of a reasonable design model deduced from laboratory estimations to maintain an industrial level throughput for the desired product. We discuss below the usefulness of our transport model for benzene in NaX to predict preliminary design criteria for scale-up operation.

In Figure 12, using our loading-dependent transport model, we predict the effect of p_{permeate} on the benzene flux across a $15 \mu\text{m}$ thick NaX membrane for $T = 493.15$ and 533.15 K and $p_{\text{feed}} = 100$ and 1000 kPa , respectively. The Maxwell–Stefan diffusivities for these conditions have been extrapolated as before from our MD simulations of benzene in NaX (section II) whereas the sorption isotherm data have been obtained by fitting the relevant experimental data of Dzhigit et al.⁹⁵ to the Langmuir isotherm. The behavior of the membrane flux under these conditions is similar to the trends observed earlier (section III.A), where the driving force effect controls the reduction in flux with permeate partial pressure, whereas the tendency of Γ and $\Theta_{\text{sat}}(T)$ dominates to decrease the flux with temperature due to a decrease in benzene loading with temperature. We observe that by maintaining significant driving forces across the membrane ($\sim 1000 \text{ kPa}$), reasonably high fluxes of $O(100 \text{ mmol}/(\text{m}^2\cdot\text{s}))$ have been predicted across the membranes. Such fluxes translate into a reasonable membrane area of $\sim 1000 \text{ m}^2$ to maintain a target benzene productivity of $300\,000 \text{ tons per year}$.⁹⁶

This rough analysis above deserves further comment. The accuracy of the predicted membrane area depends on several factors: (a) the observed discrepancy between predicted and experimental fluxes (section III.D) may render the predicted membrane area to be an underestimate; (b) more permeable supports (as compared to those used in the experiments of

Nikolakakis et al.¹⁸) should be available so that support resistances are indeed negligible in practice; (c) the observance that high membrane fluxes are not always associated with low selectivities, which not only is in contrast with what has been the observed norm for mixture permeation in laboratory studies^{18,47} but also suggests that suitable operating conditions may be chosen to simultaneously optimize flux and selectivity. Although a thorough economic feasibility analysis is not the focus of this work, an estimate of a useful design parameter (i.e., membrane surface area) from our predictions augurs well for the future of using industrial zeolite membranes for separating mixtures of saturated and unsaturated hydrocarbons.

V. Conclusions and Future Work

We applied the loading- and temperature-dependent Maxwell–Stefan (alternatively cooperative) diffusion coefficients for benzene in NaX generated by high-temperature MD simulations (see preceding companion article) in a simple membrane transport model to predict benzene fluxes in ideal single-crystal NaX membranes. Contrary to choosing approximations such as a concentration-independent Fickian diffusivity^{2,55} or a concentration-independent Maxwell–Stefan diffusivity,^{52,54–56} we make use of the Maxwell–Stefan diffusivities directly estimated from high-temperature MD simulations to predict macroscopic membrane fluxes.

We find that experimental flux trends predicted as a function of variables such as temperature, feed, and permeate side benzene partial pressures are well reproduced by our transport model and are generally governed by the coupled effects of $\Theta_{\text{sat}}(T)$, $D^{\text{MS}}(\theta, T)$, $\Gamma(\theta, T)$, and $\Delta\Theta_{\text{net}}$. We observe a flux maximum with temperature for benzene in NaX from our model predictions, a prediction we plan to test in upcoming experiments. We also find good qualitative agreement between our simulated and reported experimental flux behavior for benzene in NaX and NaY. Considering that we simulated diffusion in single-crystal NaX, whereas experimental fluxes resulted from permeation through complex, disordered polycrystalline membranes, the level of quantitative agreement is remarkable. These simulations thus serve as a quality-test for ideal membrane performance. The comparison between experiment and simulation brings forth two challenging questions: (1) Is it possible to prepare “close to ideal” zeolite membranes on less-resistive and more permeable supports? (2) Is it possible to incorporate experimental artifacts in the model development hierarchy? Our model predictions further suggest that sufficiently high fluxes across membranes, i.e., $O(100 \text{ mmol}/(\text{m}^2\cdot\text{s}))$, can be obtained by maintaining significant driving forces across the membrane at industrially relevant operating conditions.

In future experimental work, we plan to perform membrane permeation experiments spanning a wider range of loadings across the membrane thickness. These will allow us to evaluate the extended applicability of this transport model equipped with our MD simulated diffusivities. Such methodologies may warrant the use of vacuum conditions for the permeate side of the membrane. Exploring such boundary conditions in the experiments may provide further insights into interesting permeation behavior (e.g., flux maxima with temperature) in cationic guest–zeolite membrane systems and thereby understand membrane permeation better. Future simulation work will focus on predicting experimental adsorption isotherms for the benzene–FAU system, and developing models of transport through disordered membranes to elucidate the kinds of defects that ultimately influence and even control permeation through zeolite membranes.

Acknowledgment. We gratefully acknowledge generous funding from the Department of Energy (DE-FG02-94ER14485), the National Science Foundation (NSF CTS-0091406), and the National Environmental Technology Institute (NETI) for supporting research on diffusion in zeolites. We also thank the reviewers for their comments and suggestions.

References and Notes

- Pohl, P. I.; Heffelfinger, G. S.; Smith, D. M. *Mol. Phys.* **1996**, *89*, 1725.
- Vroon, Z. A. E. P.; Keizer, K.; Gilde, M. J.; Verweij, H.; Burggraaf, A. J. *J. Membr. Sci.* **1996**, *113*, 293.
- Takaba, H.; Koshita, R.; Mizukami, K.; Oumi, Y.; Ito, N.; Kubo, M.; Fahmi, A.; Miyamoto, A. *J. Membr. Sci.* **1997**, *134*, 127.
- Sholl, D. S. *Ind. Eng. Chem. Res.* **2000**, *39*, 3737.
- Mizukami, K.; Kobayashi, Y.; Morito, H.; Takami, S.; Kubo, M.; Belosludov, R.; Miyamoto, A. *Jpn. J. Appl. Phys. Part 1—Reg. Pap. Short Notes Rev. Pap.* **2000**, *39*, 4385.
- Arya, G.; Chang, H. C.; Maginn, E. J. *J. Chem. Phys.* **2001**, *115*, 8112.
- Makrodimitris, K.; Papadopoulos, G. K.; Theodorou, D. N. *J. Phys. Chem. B* **2001**, *105*, 777.
- Kobayashi, Y.; Takami, S.; Kubo, M.; Miyamoto, A. *Fluid Phase Equilib.* **2002**, *194*, 319.
- Zhang, Y.; Furukawa, S.; Nitta, T. *Sep. Purif. Technol.* **2003**, *32*, 215.
- Furukawa, S.; Nitta, T. *J. Chem. Eng. Jpn.* **2003**, *36*, 313.
- Nelson, P. H.; Auerbach, S. M. *Chem. Eng. J.* **1999**, *74*, 43.
- Gergidis, L. N.; Theodorou, D. N. *J. Phys. Chem. B* **1999**, *103*, 3380.
- van de Graaf, J. M.; Kapteijn, F.; Moulijn, J. A. *AICHE J.* **1999**, *45*, 497.
- Suzuki, S.; Takaba, H.; Yamaguchi, T.; Nakao, S. *J. Phys. Chem. B* **2000**, *104*, 1971.
- Ciavarella, P.; Moueddeb, H.; Miachon, S.; Fiary, K.; Dalmon, J. A. *Catal. Today* **2000**, *56*, 253.
- Kapteijn, F.; Moulijn, J. A.; Krishna, R. *Chem. Eng. Sci.* **2000**, *55*, 2923.
- Krishna, R.; Paschek, D. *Sep. Purif. Technol.* **2000**, *21*, 111.
- Nikolakakis, V.; Xomeritakis, G.; Abibi, A.; Dickson, M.; Tsapatsis, M.; Vlachos, D. G. *J. Membr. Sci.* **2001**, *184*, 209.
- Mizukami, K.; Takaba, H.; Kobayashi, Y.; Oumi, Y.; Belosludov, R. V.; Takami, S.; Kubo, M.; Miyamoto, A. *J. Membr. Sci.* **2001**, *188*, 21.
- Chandross, M.; Webb, E. B.; Grest, G. S.; Martin, M. G.; Thompson, A. P.; Roth, M. W. *J. Phys. Chem. B* **2001**, *105*, 5700.
- Martin, M. G.; Thompson, A. P.; Nenoff, T. M. *J. Chem. Phys.* **2001**, *114*, 7174.
- Bowen, T. C.; Falconer, J. L.; Noble, R. D.; Skoulidas, A. I.; Sholl, D. S. *Ind. Eng. Chem. Res.* **2002**, *41*, 1641.
- Kobayashi, Y.; Takami, S.; Kubo, M.; Miyamoto, A. *Desalination* **2002**, *147*, 339.
- Vareltzis, P.; Kikkinides, E. S.; Georgiadis, M. C. *Chem. Eng. Res. Design* **2003**, *81*, 525.
- Nagumo, R.; Takaba, H.; Nakao, S. *J. Phys. Chem. B* **2003**, *107*, 14422.
- Krishna, R.; Baur, R. *Sep. Purif. Technol.* **2003**, *33*, 213.
- Krishna, R.; Baur, R. *Sep. Purif. Technol.*, in press.
- Skoulidas, A. I.; Bowen, T. C.; Doelling, C. M.; Falconer, J. L.; Noble, R. D.; Sholl, D. S. *J. Membr. Sci.* **2003**, *227*, 123.
- Furukawa, S.; Goda, K.; Zhang, Y.; Nitta, T. *J. Chem. Eng. Jpn.* **2004**, *37*, 67.
- Pohl, P. I.; Heffelfinger, G. S. *J. Membr. Sci.* **1999**, *155*, 1.
- Auerbach, S. M. *Int. Rev. Phys. Chem.* **2000**, *19*, 155.
- Krishna, R.; Paschek, D. *Ind. Eng. Chem. Res.* **2000**, *39*, 2618.
- Krishna, R.; Paschek, D. *J. Phys. Chem. Chem. Phys.* **2001**, *3*, 453.
- Tunca, C.; Ford, D. M. *J. Phys. Chem. B* **2002**, *106*, 10982.
- Kita, H.; Horii, K.; Ohtoshi, Y.; Tanaka, K.; Okamoto, K. I. *J. Mater. Sci. Lett.* **1995**, *14*, 206.
- Chen, X. B.; Yang, W. S.; Liu, J.; Xu, X. C.; Huang, A. S.; Lin, L. W. *J. Mater. Sci. Lett.* **2002**, *21*, 1023.
- Mohammadi, T.; Pak, A. *Microporous Mesoporous Mater.* **2002**, *56*, 81.
- Cheng, Z. L.; Chao, Z. S.; Fang, W. P.; Wan, H. L. *J. Inorg. Mater.* **2003**, *18*, 1306.
- Li, Y.; Wang, X.; Zhang, S. G.; Wang, D. W. *Trans. Nonferrous Met. Soc. China* **2003**, *13*, 55.
- Murad, S.; Jia, W.; Krishnamurthy, M. *Chem. Phys. Lett.* **2003**, *369*, 402.
- van den Berg, A. W. C.; Gora, L.; Jansen, J. C.; Maschmeyer, T. *Microporous Mesoporous Mater.* **2003**, *66*, 303.
- Chen, X. B.; Yang, W. S.; Liu, J.; Lin, L. W. *J. Mater. Sci.* **2004**, *39*, 671.
- Xu, X. C.; Yang, W. S.; Liu, J.; Lin, L. W.; Stroh, N.; Brunner, H. *J. Membr. Sci.* **2004**, *229*, 81.
- Hasegawa, Y.; Kusakabe, K.; Morooka, S. *Chem. Eng. Sci.* **2001**, *56*, 4273.
- Nair, S.; Lai, Z. P.; Nikolakis, V.; Xomeritakis, G.; Bonilla, G.; Tsapatsis, M. *Microporous Mesoporous Mater.* **2001**, *48*, 219.
- Jeong, B. H.; Hasegawa, Y.; Sotowa, K.; Kusakabe, K.; Morooka, S. *J. Chem. Eng. Jpn.* **2002**, *35*, 167.
- Jeong, B.-H.; Hasegawa, Y.; Kusakabe, K.; Morooka, S. *Sep. Sci. Technol.* **2002**, *37*, 1225.
- Jeong, B. H.; Hasegawa, Y.; Sotowa, K. I.; Kusakabe, K.; Morooka, S. *J. Membr. Sci.* **2003**, *213*, 115.
- Kamat, M.; Dang, W. J.; Keffer, D. *J. Phys. Chem. B* **2004**, *108*, 376.
- Kita, H.; Fuchida, K.; Horita, T.; Asamura, H.; Okamoto, K. *Sep. Purif. Technol.* **2001**, *25*, 261.
- Onsager, L. *Phys. Rev.* **1931**, *37*, 405.
- Krishna, R. *Chem. Eng. Sci.* **1990**, *45*, 1779.
- Krishna, R. *Chem. Eng. Sci.* **1993**, *48*, 845.
- Krishna, R.; Van den Broeke, L. J. P. *Chem. Eng. J. Biochem. Eng. J.* **1995**, *57*, 155.
- Kapteijn, F.; Bakker, W. J. W.; Zheng, G.; Poppe, J.; Moulijn, J. A. *The Chem. Eng. J. Biochem. Eng. J.* **1995**, *57*, 145.
- Vandenbroeke, L. J. P. *AICHE J.* **1995**, *41*, 2399.
- Keil, F. J.; Krishna, R.; Coppens, M. O. *Rev. Chem. Eng.* **2000**, *16*, 71.
- Krishna, R. Modeling issues in zeolite applications. In *Handbook of Zeolite Science and Technology*; Dutta, P. K., Ed.; Marcel-Dekker: New York, 2003; p 1105.
- Karger, J.; Vasenkov, S.; Auerbach, S. M. Diffusion in zeolites. In *Handbook of Zeolite Science and Technology*; Dutta, P. K., Ed.; Marcel-Dekker: New York, 2003; p 341.
- Harikrishnan, R.; Auerbach, S. M. Modeling Jump Diffusion in Zeolites: I. Principles and Methods. In *NATO-ASI Series C: Fluid Transport in Nanopores*; Fraissard, J., Conner, W. C., Eds.; Kluwer Academic Publishers: Dordrecht: The Netherlands (in press).
- Maginn, E. J.; Bell, A. T.; Theodorou, D. N. *J. Phys. Chem.* **1993**, *97*, 4173.
- Theodorou, D. N.; Snurr, R. Q.; Bell, A. T. Molecular dynamics and diffusion in microporous materials. In *Comprehensive Supramolecular Chemistry*; Bein, T., Ed.; Pergamon Press: Oxford, U.K., 1996; Vol. 7, p 507.
- Krishna, R.; Wesselingh, J. A. *Chem. Eng. Sci.* **1997**, *52*, 861.
- Van Den Broeke, L. J. P. The Maxwell–Stefan Theory for Micropore Diffusion. Ph.D. Thesis, Universiteit van Amsterdam, 1994.
- Kapteijn, F.; Bakker, W. J. W.; van de Graaf, J.; G., Z.; Poppe, J.; Moulijn, J. A. *Catal. Today* **1995**, *25*, 213.
- Burggraaf, A. J. *J. Membr. Sci.* **1999**, *155*, 45.
- Gardner, T. Q.; Flores, A. I.; Noble, R. D.; Falconer, J. L. *AICHE J.* **2002**, *48*, 1155.
- Ruthven, D. M.; Doetsch, I. H. *AICHE J.* **1976**, *22*, 882.
- Krishna, R. *Gas Sep. Purif.* **1993**, *7*, 91.
- van de Graaf, J. M.; Kapteijn, F.; Moulijn, J. A. *J. Membr. Sci.* **1998**, *144*, 87.
- Farooq, S.; Karimi, I. A. *J. Membr. Sci.* **2001**, *186*, 109.
- Paschek, D.; Krishna, R. *Phys. Chem. Chem. Phys.* **2000**, *2*, 2389.
- Krishna, R.; Paschek, D. *Chem. Eng. J.* **2002**, *87*, 1.
- Fuller, E. N.; Schettler, P. D.; Giddings, J. C. *Ind. Chem. Eng.* **1966**, *58*, 19.
- Auerbach, S. M.; Jousse, F.; Vercauteren, D. P. Dynamics of Sorbed Molecules in Zeolites. In *Computer Modelling of Microporous and Mesoporous Materials*; Catlow, C. R. A., van Santen, R. A., Smit, B., Eds.; Elsevier: Amsterdam, 2004; p 49.
- Elfert, K.; Rosenkranz, H. J.; Rudolf, H. Separation of aromatic hydrocarbons from mixtures, using polyurethane membranes. In US patent Number 4,115,465; Bayer Aktiengesellschaft (Leverkusen, DE1), 1978.
- Yamaguchi, T.; Nakao, S.; Kimura, S. *J. Macromolecules* **1991**, *24*, 5522.
- Ruckenstein, E.; Sun, F. M. *Ind. Eng. Chem. Res.* **1995**, *34*, 3581.
- Kusakabe, K.; Yoneshige, S.; Morooka, S. *J. Membr. Sci.* **1998**, *149*, 29.
- Villaluenga, J. P. G.; Tabe-Mohammadi, A. *J. Membr. Sci.* **2000**, *169*, 159.
- Cunha, V. S.; Paredes, M. L. L.; Borges, C. P.; Habert, A. C.; Nobrega, R. *J. Membr. Sci.* **2002**, *206*, 277.
- Sakaguchi, T.; Yumoto, K.; Kwak, G.; Yoshikawa, M.; Masuda, T. *Polym. Bull.* **2002**, *48*, 271.
- Razdan, U.; Joshi, S. V.; Shah, V. J. *Curr. Sci.* **2003**, *85*, 761.
- Yoshikawa, M.; Matsumoto, M.; Igarashi, Y. *J. Appl. Polym. Sci.* **2003**, *88*, 183.

- (85) Wang, Y. C.; Li, C. L.; Huang, J.; Lin, C.; Lee, K. R.; Liaw, D. J.; Lai, J. Y. *J. Membr. Sci.* **2001**, *185*, 193.
- (86) Yamasaki, A.; Shinbo, T.; Mizoguchi, K. *J. Appl. Polym. Sci.* **1997**, *64*, 1061.
- (87) Yildirim, A. E.; Hilmioglu, N. D.; Tulbentci, S. *Chem. Eng. Technol.* **2001**, *24*, 275.
- (88) Yoshikawa, M.; Tsubouchi, K. *J. Membr. Sci.* **1999**, *158*, 269.
- (89) Pithan, F.; Staudt-Bickel, C.; Hess, S.; Lichtenthaler, R. N. *ChemPhysChem* **2002**, *3*, 856.
- (90) Fang, J. H.; Tanaka, K.; Kita, H.; Okamoto, K. *Polymer* **1999**, *40*, 3051.
- (91) Inui, K.; Miyata, T.; Uragami, T. *J. Polym. Sci. Part B—Polym. Phys.* **1998**, *36*, 281.

- (92) Cunha, V. S.; Nobrega, R.; Habert, A. C. *Brazilian J. Chem. Eng.* **1999**, *16*, 297.
- (93) Brandani, S.; Xu, Z.; Ruthven, D. *Microporous Mater.* **1996**, *7*, 323.
- (94) Jeong, B. H.; Hasegawa, Y.; Kusakabe, K.; Morooka, S. *Sep. Sci. Technol.* **2002**, *37*, 1225.
- (95) Dzhigit, O. M.; Kiselev, A. V.; Rachmanova, T. A. *Zeolites* **1984**, *4*, 389.
- (96) www.highbeam.com/library/. LG-Caltex Completes World's Largest Benzene-Toluene Plant, 2000.